



1 **Effects of seasonal variations in vegetation and precipitation on** 2 **catchment erosion rates along a climate and ecological gradient:** 3 **Insights from numerical modelling**

4 Hemanti Sharma¹ and Todd A. Ehlers¹

5 ¹Department of Geosciences, University of Tübingen, Schnarrenbergstr. 94-96, 72076, Germany

6 *Correspondence to:* Todd A. Ehlers (todd.ehlers@uni-tuebingen.de)

7 **Abstract.** Precipitation in wet seasons influences catchment erosion and contributes to annual erosion rates. However, wet
8 seasons are also associated with increased vegetation cover, which helps resist erosion. This study investigates the effect of
9 present-day seasonal variations in rainfall and vegetation cover on erosion rates for four catchments along the extreme climate
10 and ecological gradient (from arid to temperate) of the Chilean Coastal Cordillera (~26 °S – ~38 °S). We do this using the
11 Landlab-SPACE landscape evolution model modified to account for vegetation-dependent hillslope-fluvial processes and
12 hillslope hydrology. Model inputs include present-day (90 m) topography, and a timeseries (from 2000-2019) of MODIS-
13 derived NDVI for vegetation seasonality; weather station observations of precipitation; and evapotranspiration obtained from
14 GLDAS NOAA. Simulations were conducted with a step-wise increase in complexity to quantify the sensitivity of catchment
15 scale erosion rates to seasonal variations in precipitation and/or vegetation cover. Simulations were conducted for 1,000 years
16 (20 years of vegetation and precipitation observations repeated 50 times). After detrending the results for long-term transient
17 changes, the last 20 years were analyzed. Results indicate that when vegetation cover is varied but precipitation is held constant,
18 the amplitude of change in erosion rates relative to mean erosion rates ranges between 6.5% (humid-temperate) to 36%
19 (Mediterranean setting). In contrast, in simulations with variable precipitation change and constant vegetation cover, the
20 amplitude of change in erosion rates is higher and ranges between 13% (arid) to 91% (Mediterranean setting). Finally,
21 simulations with coupled precipitation and vegetation cover variations demonstrate variations in catchment erosion of 13%
22 (arid) to 97% (Mediterranean setting). Taken together, we find that precipitation variations more strongly influence seasonal
23 variations in erosion rates. However, the effects of seasonal variations in vegetation cover on erosion are also significant
24 (between 5-36%) and are most pronounced in semi-arid to Mediterranean settings and least prevalent in arid and humid-
25 temperature settings.

26 **Keywords:** Landlab, vegetation, Chilean Coastal Cordillera, biogeomorphology, seasonality, precipitation.

27 **1 Introduction**

28 Catchment erosion rates vary spatially and temporally (e.g., Wang et al., 2021) and depend on topography (slope, Carretier et
29 al., 2018) vegetation cover and type (e.g., Zhang et al., 2011; Starke et al., 2020; Schaller and Ehlers, 2022) and precipitation
30 rates (e.g., Cerdà, 1998; Tucker and Bras, 2000). Over annual timescales, temporal variations in catchment erosion occur in
31 response to seasonal variations in precipitation and vegetation cover. For example, previous work has found that a significant
32 fraction of annual erosion occurs during wet seasons, with high runoff rates (Hancock and Lowry, 2021; Leyland et al., 2016;
33 Gao et al., 2021; Wulf et al., 2010). However, this increase in precipitation during wet seasons also promotes vegetation
34 growth, which in turn influences erosion rates (Langbein and Schumm, 1958; Zheng, 2006; Schmid et al., 2018). Seasonality,
35 and longer-term, changes in both precipitation and vegetation cover plays a crucial role in intra-annual changes in erosion rates
36 (Istanbuluoglu and Bras, 2006; Yetemen et al., 2015; Schmid et al., 2018; Sharma et al., 2021). The intensity, frequency, and
37 seasonality of precipitation and vegetation cover change within a year depend on the climate and ecological conditions of the
38 area of interest (Herrmann and Mohr, 2011). One means of investigating the effects of seasonality in precipitation and (or)



39 vegetation cover on erosion rates is through landscape evolution modeling (LEM), which can be parameterized for variations
40 in vegetation-dependent hillslope and fluvial processes over seasonal time scales.

41 Previous modeling and observational studies have investigated the effects of seasonality in precipitation and vegetation on
42 catchment erosion. Bookhagen et al., (2005), Wulf et al., (2010), and Deal et al., (2017) investigated the effects of stochastic
43 variations in precipitation on erosion and sediment transport in the Himalayas. They found that high variability in rainstorm
44 days (>80% of MAP) during the wet season (summer monsoon) caused high variability in the suspended sediment load. Work
45 by Chakrapani (2005) identifies the control of mean local relief and seasonality in precipitation on sediment load in rivers.
46 Similar seasonality in sediment loads was reported in a field study in Iran, using sediment traps and erosion pins. These authors
47 concluded that wet seasons have maximum erosion rates (>70% of annual), which decreases in the dry season (<10% of annual)
48 (Mosaffaie et al., 2015). Field observations in the heavily vegetated Columbian Andes concluded that soil erosion and nutrient
49 losses are significantly influenced by precipitation seasonality (Suescún et al., 2017). In contrast, work by Steegen et al., (2000)
50 in a loamy agricultural catchment in central Belgium found suspended sediment concentrations in streams were lower during
51 summer (wet) rather than winter (dry) months due to the development in vegetation cover in the wet season. Other workers
52 have found a dependence of seasonal erosion on ecosystem type. For example, Istanbuloglu et al., (2006) found a reduction
53 in soil loss potential to storm frequency in humid ecosystems compared to arid and semi-arid regions. Work by Wei et al.,
54 (2015) documented that differences in vegetation cover may contribute to long-term erosion and sedimentation. However,
55 seasonal variations in runoff and sediment yield are mainly influenced by intra-annual rainfall variations. Finally, previous
56 work in a Mediterranean environment (Gabarrón-Galeote et al., (2013) described rainfall intensity as the main factor in
57 determining hydrological erosive response, regardless of the rainfall depth of an event.

58 When looking at seasonal vegetation changes in more detail, several different studies suggest these changes are important for
59 catchment erosion. For example, Garatuza-Payán et al., (2005) emphasized that seasonal patterns in erosion are strongly
60 influenced by plant phenology demonstrated by the changes in vegetation cover (as measured by NDVI). A similar study on
61 the Loess Plateau, China, by Zheng (2006) documented decreasing soil erosion as vegetation cover increases during the wet
62 season. Work conducted in a forested setting (Zhang et al., 2014) documented the importance of tree cover as an effective
63 filter for decreasing the effects of rainfall intensity on soil structure, runoff, and sediment yield. Numerical modeling studies
64 have also found a significant impact of vegetation on erosion. For example, Zhang et al., (2019) found that when precipitation
65 is kept constant, the effect of vegetation cover change on sediment yields is significant (20-30% of the total flux). Also, during
66 the early to the mid-wet season, the richness and evenness of plant cover play an essential role in reducing erosion rates during
67 low rainfall events (Hou et al., 2020). However, in the case of high-intensity rainfall events at the start of a wet season, when
68 vegetation cover is low, the duration and intensity of rainfall were found to significantly affect erosion rates (Hancock and
69 Lowry, 2015). Other work conducted in a Mediterranean environment points to the coincidence of peak rainfall erosivity in
70 low vegetation cover settings, leading to an increased risk of soil erosion (Ferreira and Panagopoulos, 2014). Despite
71 potentially conflicting results in the previous studies, what is clear is that seasonality in precipitation and vegetation covers are
72 co-conspire to influence catchment erosion, although which factor (precipitation or vegetation) plays the dominant role is
73 unclear.

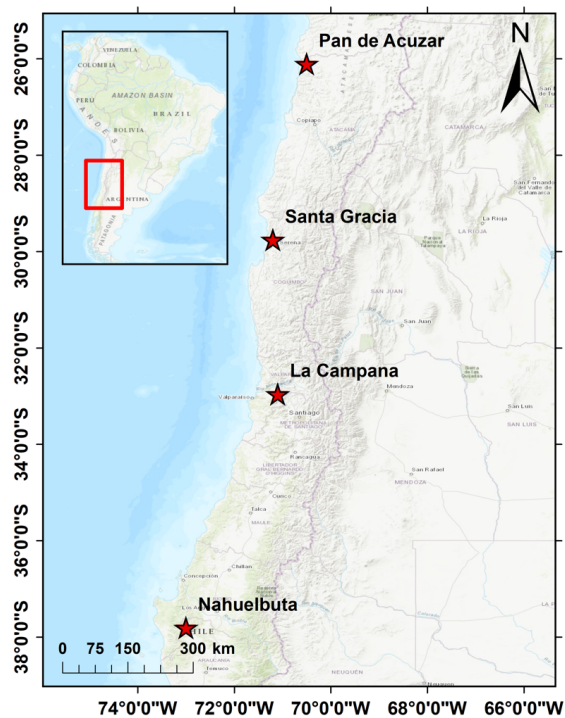
74 This study complements the previous work by applying a Landscape Evolution Model (LEM) to investigate seasonal transients
75 in catchment erosion due to variations in precipitation and vegetation. We do this for four locations in the extreme climate and
76 ecological gradient (i.e., arid, semi-arid, Mediterranean, and humid temperate) of the Chilean Coastal Cordillera. Our efforts
77 are focused on testing two hypotheses: (1) if precipitation is the first-order driver of seasonal erosion rates, then the influence
78 of seasonal changes in vegetation cover would be of low significance, and (2) catchment erosion in arid and semi-arid regions
79 is more sensitive to seasonality in precipitation and vegetation than the Mediterranean and humid temperate regions. To test
80 the above hypotheses, we conduct a sensitivity analysis of fluvial and hillslope erosion over four Chilean study areas to
81 investigate the individual effects of seasonal changes in vegetation cover and precipitation compared to simulations with



82 coupled variations in precipitation and vegetation cover. We do this using a two-dimensional LEM (the Landlab-SPACE
83 software), which explicitly handles bedrock and sediment entrainment and deposition. We build upon the approach of Sharma
84 et al., (2021) with the additional consideration of soil-water infiltration. Our model setup is focused on present conditions in
85 the Chilean Coastal Cordillera (Fig. 1) and use as input present day topography from SRTM DEMs (90 m) for four regions
86 with different climate/ecological settings. Simulations in these different ecosystems are drive by observed variations vegetation
87 cover from MODIS NDVI (between 2000 – 2019) and observed precipitation rates over the same time period from neighboring
88 weather stations.

89 2 Study Areas

90 This section summarizes the geologic, climate, and vegetation settings of the four selected catchments (Fig. 1) investigated in
91 the Chilean Coastal Cordillera. These catchments (from north to south) are located in the Pan de Azúcar National Park (arid,
92 ~26°S), Santa Gracia nature preserve (semi-arid, ~30°S), and the La Campana (mediterranean, ~33°S) and Nahuelbuta
93 (temperate-humid, ~38°S) national parks. Together, these study areas span ~1,300 km distance of the Coastal Cordillera. These
94 study areas are chosen for their steep climate and ecological gradient from North (arid environment with small shrubs) to South
95 (humid temperate environment with evergreen mixed forests) (Schaller et al., 2020). The study areas are part of the German-
96 Chilean priority research program EarthShape (www.earthshape.net) and ongoing research efforts within these catchments.



97
98 **Figure 1.** Study areas in the Coastal Chilean Cordillera ranging from an arid environment in the North (Pan de
99 Azúcar), semi-arid (Santa Gracia), Mediterranean (La Campana), and humid temperate environment in the South
100 (Nahuelbuta). The above map is obtained from the Environmental System Research Institute (ESRI) map server
101 (https://services.arcgisonline.com/ArcGIS/rest/services/World_Topo_Map/MapServer, last access: 25 April 2022).

102 The bedrock of the four study areas is composed of granitoid rocks, including granites, granodiorites, and tonalites in Pan de
103 Azúcar, La Campana, and Nahuelbuta, respectively and gabbro and diorites in Santa Gracia (Oeser et al., 2018). The soil types



104 in each catchment were identified as a sandy loam in three northern catchments (with high bulk density: $1300 - 1500 \text{ kg m}^{-3}$)
105 and sandy clay loam in Nahuelbuta (with lower bulk density: 800 kg m^{-3}) (Bernhard et al., 2018). The western margin of Chile
106 along the latitudes of the different study areas is characterized by a similar tectonic setting whereby an oceanic plate (currently
107 the Nazca plate) has been subducting under the South American plate since the Palaeozoic. Despite this common tectonic
108 setting along, slight differences in modern rock uplift rates are documented in the regions surrounding the three northern
109 catchments (i.e., $< 0.1 \text{ mm yr}^{-1}$ for $\sim 26^\circ\text{S}$ to $\sim 33^\circ\text{S}$) (Melnick, 2016) and the southern catchment (i.e., 0.04 to $> 0.2 \text{ mm yr}^{-1}$
110 for $\sim 38^\circ\text{S}$ over the last $4 \pm 1.2 \text{ Ma}$) (Glodny et al., 2008; Melnick et al., 2009). Over geologic (millennial) timescales, measured
111 denudation rates in the region range between ~ 0.005 to $\sim 0.6 \text{ mm yr}^{-1}$ (Schaller et al., 2018). To facilitate a comparison between
112 the study areas and focus on erosion variations from seasonal changes in precipitation and vegetation, we assume a uniform
113 rock uplift rate of 0.05 mm yr^{-1} for this study. This rate is broadly consistent with the range of previously reported values.
114 The climate gradient in the study areas ranges from an arid climate in Pan de Azúcar (north) with mean annual precipitation
115 (MAP) of $\sim 11 \text{ mm yr}^{-1}$ to semi-arid in Santa Gracia (MAP: $\sim 88 \text{ mm yr}^{-1}$), the Mediterranean in La Campana (MAP: $\sim 350 \text{ mm}$
116 yr^{-1}), and a temperate-humid climate in Nahuelbuta (south) with a MAP of 1400 mm yr^{-1} (Ziese et al., 2020). The observed
117 mean annual temperatures (MAT) also vary with latitude ranging from $\sim 20^\circ\text{C}$ in the north to $\sim 5^\circ\text{C}$ in the south (Übernicker et
118 al., 2020). The previous gradients in MAP and MAT and latitudinal variations in solar radiation result in a southward increase
119 in vegetation density (Bernhard et al., 2018). The vegetation gradient evident from mean MODIS Normalized Difference
120 Vegetation Index (NDVI) values range from ~ 0.1 in Pan de Azúcar (north) to ~ 0.8 in Nahuelbuta (south) (Didan, Kamel,
121 2015). In this study, NDVI values are used as a proxy for vegetation cover density, similar to the approach of Schmid et al.
122 (2018).
123 This gradient in climate and vegetation cover from north to south in the Chilean Coastal Cordillera provides an opportunity to
124 study the effects of seasonal variations in vegetation cover and precipitation on catchment-scale erosion rates in different
125 environments.

126 3 Methods

127 This section comprises a description of model inputs (section 3.1), estimation of runoff rates (section 3.2), model setup (section
128 3.3), and initial and boundary conditions (section 3.4). This is followed by an overview of simulations conducted (section 3.5)
129 and a brief description of how detrending the model results was conducted to remove long-term transients (section 3.6).

130 3.1 Data used for model inputs

131 In contrast to previous modeling studies (Schmid et al., 2018; Sharma et al., 2021) in the same regions, we used present-day
132 topography as the initial condition for simulations instead of a synthetic topography produced during a model spin-up phase
133 in LandLab. Initial topography for the four selected catchments was obtained by cropping the SRTM digital elevation model
134 (DEM) in rectangular shapes encapsulating the catchment of interest (Fig. 1). These catchments are same as those investigated
135 with previous soil, denudation, and geophysical studies (e.g., Bernhard et al., 2018; Oeser et al., 2018; Schaller et al., 2018;
136 Dal Bo et al., 2019). The DEM has a spatial resolution of 90 m and is the same as the cell size used in the model (dx and dy)
137 (SRTM data set of Earth Resources Observation And Science (EROS) Center, 2017). Maximum relief of $\sim 1852 \text{ m}$ is observed
138 in La Campana ($\sim 33^\circ\text{S}$), followed by $\sim 1063 \text{ m}$ in Santa Gracia ($\sim 30^\circ\text{S}$), $\sim 809 \text{ m}$ in Nahuelbuta ($\sim 38^\circ\text{S}$) and $\sim 623 \text{ m}$ Pan de
139 Azúcar ($\sim 26^\circ\text{S}$). Catchment sizes considered vary between $\sim 64 \text{ km}^2$ in Pan de Azúcar, $\sim 142.5 \text{ km}^2$ in Santa Gracia, ~ 106.8
140 km^2 in La Campana and $\sim 68.7 \text{ km}^2$ in Nahuelbuta. We note that present-day topography as the initial condition in simulations
141 can introduce an initial transient in erosion rates due to model erosional parameters (e.g., erodibility, hillslope diffusivity)
142 differing from actual parameters within the catchment, we address this issue through a detrending of model results described
143 later.



144 Precipitation data applied over each study area (Fig. 3b) was acquired from the Global Precipitation Climatology Centre
145 (GPCC) for the period 01/03/2000 to 31/12/2019 (DD/MM/YEAR). The data has a spatial resolution of 1° (~111 km) and a
146 1-day temporal resolution and comprises daily land-surface precipitation from rain gauges built on Global Telecommunication
147 System-based and historic data (Ziese et al., 2020). The previous data was augmented with daily precipitation weather station
148 data from 01/02/2020 to 28/02/2020 obtained from Übernickel et al., (2020). We do this to include all the seasons between
149 2000 to 2019, i.e., from the Austral Autumn of 2000 to the Austral Summer of 2019. The periods (months of a year) of specific
150 seasons in the Chilean Coastal Cordillera are illustrated in Table 1. Seasonal precipitation rates were calculated by summing
151 up daily precipitation rates at three-month intervals. The seasonality and intensity of precipitation in the wet season (winter)
152 increases from the arid (Pan de Azúcar) to humid temperate (Nahuelbuta) region.

153 **Table 1. Months of a year corresponding to specific seasons in the Chilean Coastal Cordillera**

Seasons	Months
Summer ^{d*}	December - February
Autumn ^{w*}	March - May
Winter ^{w*}	June - August
Spring ^{d*}	September - November

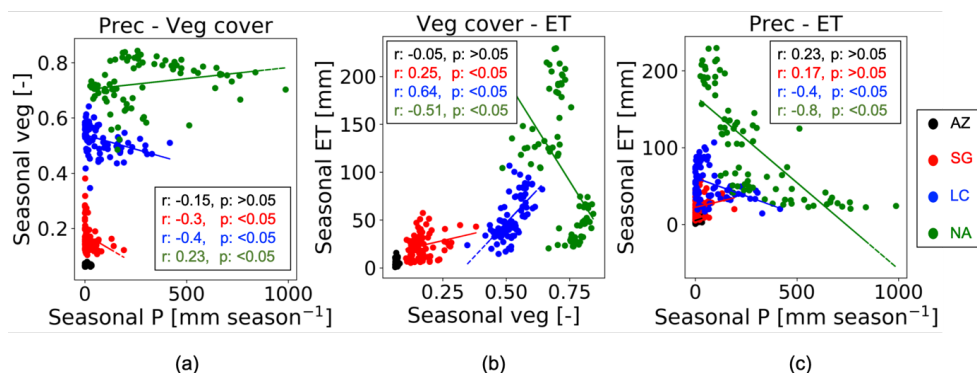
154
155

*d: dry season, w: wet season

156 NDVI derived from remote sensing imagery has been proven as an effective tool to estimate seasonal changes in vegetation
157 cover density (Garatuza-Payán et al., 2005). Normalized difference vegetation index (NDVI) values were obtained from
158 MODIS (Didan, Kamel, 2015) satellite data and were used as a proxy for changes in vegetation cover in the catchments. The
159 NDVI data were acquired for 20 years (01/03/2000 – 28/02/2020), with a spatial resolution of 250 m and temporal resolution
160 of 16 days. For application within the model simulations, the vegetation cover dataset was resampled to match the spatial
161 resolution (90 m) of SRTM DEM and temporal resolution of 3 months. To summarize, season variations in precipitation rate
162 and vegetation cover were applied to the simulations between 01/03/2000 and 28/02/2020 and encompass a 20-year record of
163 observation variations in these factors.

164 Additional aspects of the catchment hydrologic cycle were determined using the following approaches for the same time period
165 previously mentioned. First, evapotranspiration (ET) data was obtained from Global Land Data Assimilation System (GLDAS)
166 Noah version 2.1, with a monthly temporal resolution and spatial resolution of 0.25° (~28 km) (Beaudoin et al., 2020; Rodell
167 et al., 2004). The data was obtained from March-2000 to February-2020. Due to the coarse resolution of the dataset, ET is
168 assumed to be uniform over the entire catchment area. No higher resolution datasets were available over the 20-year time-
169 period of interest.

170 Soil properties such as the grain size distribution (sand, silt, and clay fraction) and bulk density were adapted from Bernhard
171 et al., (2018) to estimate soil water infiltration capacity in each study area. Based on these soil properties, the soils have been
172 classified as a sandy loam (in Pan de Azúcar, Santa Gracia, and La Campana) and sandy clay loam (Nahuelbuta). Average
173 bulk density values of 1300 kg m⁻³, 1500 kg m⁻³, 1300 kg m⁻³, and 800 kg m⁻³ were used for Pan de Azúcar, Santa Gracia, La
174 Campana, and Nahuelbuta, respectively (Bernhard et al., (2018).



175

176 **Figure 2. Parameter correlation for model input data (i.e., seasonal precipitation, vegetation cover and**
 177 **evapotranspiration) including: (a) seasonal precipitation [mm season⁻¹] and fraction of vegetation cover [-], (b)**
 178 **fractional seasonal vegetation cover [-] and evapotranspiration [mm], and (c) seasonal precipitation [mm season⁻¹] and**
 179 **evapotranspiration [mm]. The plots represent observations corresponding to Autumn of 2000 to Summer of 2019. Each**
 180 **data point represents one season and are color coded by study area (AZ: Pan de Azúcar, SG: Santa Gracia, LC: La**
 181 **Campana, and NA: Nahuelbuta).**

182 Figure 2 shows correlations between the model input data, such as variable climatic or hydrologic cycle metrics (i.e.,
 183 precipitation and evapotranspiration) and vegetation cover for each study area investigated. The relationships, and regression
 184 lines, shown for each area in different climate-ecological zones the general seasonal relationships over the 20 years (i.e.,
 185 Autumn of 2000 – Summer of 2019) of data. For example, the correlation between seasonal precipitation and vegetation cover
 186 (Fig. 2a) illustrates a moderate negative correlation ($r > -0.4$) in the semi-arid (SG) and Mediterranean (LC) regions. In contrast,
 187 vegetation in the humid temperate region (NA) is positively correlated ($r: 0.23$). ET and vegetation cover are positively
 188 correlated (Fig. 2b) in the semi-arid (SG) and Mediterranean regions (LC). However, the correlations are negative in the humid-
 189 temperate region (NA). The correlation between seasonal precipitation and ET (Fig. 2c) is slightly positive ($r: \sim 0.2$) in the
 190 semi-arid region (SG) and moderately negative ($r: -0.4$) in the Mediterranean (LC) study area. However, we observe a strong
 191 negative correlation ($r: -0.8$) between precipitation and ET in humid-temperate and Mediterranean regions (LC and NA, Fig.
 192 2c). This negative correlation is owed to the steep negative gradient in temperature (e.g., ~ 2.5 °C in NA) and solar radiation
 193 (Übernicketl et al., 2020) during winters (wet season) in southern latitudes (LC and NA).

194 3.2 Estimation of runoff rates

195 The precipitation rates [m season⁻¹] are subjected to soil-water infiltration [m season⁻¹] and evapotranspiration [m season⁻¹] to
 196 estimate the seasonal runoff rates [mm season⁻¹]. The runoff rates (R) at every time step (t) are calculated using actual soil-
 197 water infiltration (I_a) and evapotranspiration (ET) as follows,

$$198 \quad R(t) = P(t) - I_a(t) - ET(t) \quad (1)$$

199 where, P is the precipitation amount in a season. This relationship was applied in the model grid cells with non-zero sediment
 200 thickness.

201 The soil-water infiltration rate was estimated by applying the Green-Ampt equation (Green and Ampt, 1911; Julien et al.,
 202 1995):

$$203 \quad f(t) = K_e \left(1 + \frac{\psi \cdot \Delta \theta}{F} \right) \quad (2)$$



204 where $f(t)$ is the infiltration rate [m s^{-1}] at time t , K_e is the effective hydraulic conductivity [m s^{-1}], F is the cumulative infiltration
205 [m], Ψ is the suction at the wetting front [m], and $\Delta\theta$ is the difference between saturated and initial volumetric moisture content
206 [$\text{m}^3 \text{m}^{-3}$]. Effective hydraulic conductivity is highly variable and anisotropic; hence, it was considered to be uniform with a
207 value of $1 \times 10^{-6} \text{ m s}^{-1}$ for each catchment.

208 Following the approach of Istanbuluoglu and Bras, (2006) for loamy soils, the soil-water infiltration was modified to account
209 for variable vegetation cover in each grid cell, as follows:

$$210 \quad I_c(t) = f(t)(1 - V(t)) + 4f(t)(V(t)) \quad (3)$$

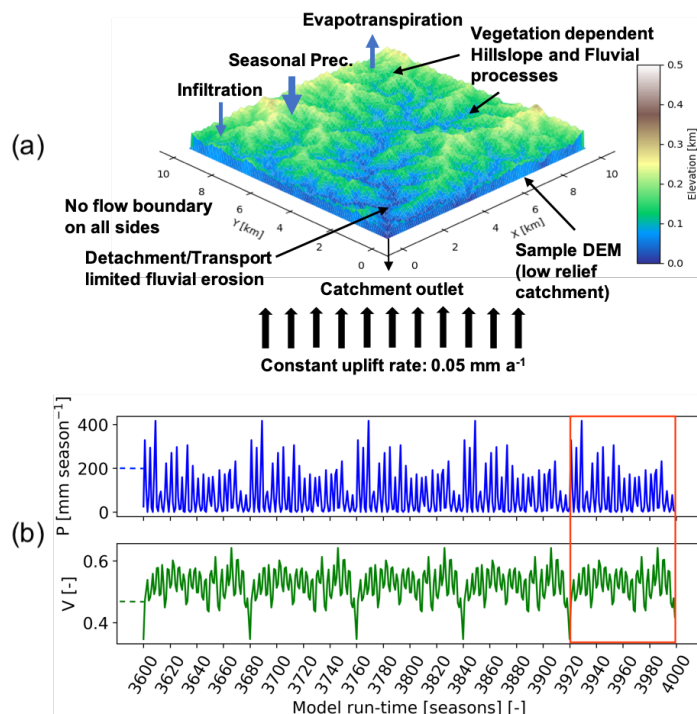
$$211 \quad I_a(t) = \text{Min}[P(t), I_c(t)] \quad (4)$$

212 where I_c is the infiltration capacity and V is the vegetation cover (between 0 and 1) in a model grid cell at time-step t . Values
213 used in the simulations for the parameters in equations 2-4 are provided in appendix Table A1.

214 3.3 Model setup

215 We applied the Landlab landscape evolution model (Hobley et al., 2017), combined with the SPACE 1.0 module of Shobe et al.
216 (2017). The SPACE module allows coupled detachment-transport limited fluvial processes with simultaneous bedrock
217 erosion and sediment entrainment/deposition. The Landlab-SPACE programs were modified for vegetation-dependent
218 hillslope processes (Johnstone and Hilley, 2014) and vegetation-dependent overland flow and fluvial erosion using the
219 approach described in Schmid et al. (2018) and Sharma et al. (2021). In addition, the geomorphic processes considered involve
220 weathering and regolith production (Barnhart et al., 2019) and infiltration of surface water into soil (Rengers et al., 2016) based
221 on the Green-Ampt method (Green and Ampt, 1911), and runoff modeling.

222 The model parameters (Table. A1) are calibrated to the distinct climate and ecological settings in the Chilean Coastal Cordillera
223 observations of Schaller et al., (2018). The model state parameters (i.e., erosion, diffusion, lithology, tectonic rock uplift rate,
224 etc.) in the simulations are adapted from Sharma et al., (2021). The model was simulated at a seasonal scale (time step of three
225 months) from the Autumn of 2000 (01/03/2000) to the Summer of 2019 (28/02/2020). Simulations were conducted for a total
226 time of 1000 years with a time-step of 1 season (3 months) with 20 years (2000 – 2019) of observations in vegetation and
227 precipitation. These 20-years of observations were repeated (looped) 50 times, to identify, and detrend, long-term transient
228 trends in catchment erosion rates due to potential differences in assumed erosional parameters such as the hillslope diffusivity
229 or fluvial erodibility. The combined effect of temporally variable (at seasonal scale) precipitation and vegetation cover (also
230 spatially variable) on catchment-scale erosion rates was therefore the primary factors influencing predicted erosion rates.



231
 232 **Figure 3. Schematic of the model geometry and seasonal precipitation and vegetation forcings used in this study. (a)**
 233 **Model setup representing sample DEM (low relief catchment) with no flow boundaries on all sides and a single**
 234 **catchment outlet. The model involves vegetation-dependent seasonal hillslope and fluvial processes and rainfall-**
 235 **infiltration-runoff modeling. (b) Seasonal precipitation and vegetation cover dataset (Mediterranean, La Campana,**
 236 **setting) for the last five iterations of model simulations. The results of highlighted iterations (after detrending for long-**
 237 **term transients) are analyzed in consecutive sections.**

238 3.4 Boundary and initial conditions

239 The boundaries are closed (no flow) on all sides, with a single stream outlet at the point of minimum elevation at boundary
 240 nodes (Fig. 3). Initial sediment cover thickness is considered uniform across the model domain, and was approximated based
 241 on observations by Schaller et al., (2018) and Dal Bo et al., (2019). The sediment thickness used are 0.2 m in arid (AZ), 0.45
 242 m in semi-arid (SG), 0.6 m in the Mediterranean (LC), and 0.7 m in humid temperate (NA) catchments. The initial rock uplift
 243 rate is kept constant throughout the entire model run as 0.05 mm yr^{-1} , adapted from a similar study (Sharma et al., 2021).

244 3.5 Overview of simulations conducted

245 The simulations were designed to identify the sensitivity of erosion rates to seasonal variations in either precipitation rates or
 246 vegetation cover, as well as the more realistic scenario of coupled seasonal variations in both vegetation cover and
 247 precipitation. We evaluated this sensitivity with a step-wise increase in model complexity. Three sets of simulations were
 248 designed for the four selected study areas, which are as follows,

- 249 1. Scenario 1: Influence of constant (mean seasonal) precipitation with seasonal variations in vegetation cover
 250 catchment-scale erosion rates.
- 251 2. Scenario 2: Influence of seasonal variation in precipitation and constant (mean seasonal) vegetation cover on
 252 catchment-scale erosion rates.



253 3. Scenario 3: Influence of coupled seasonal variations in both precipitation and vegetation cover on catchment-scale
254 erosion rates.

255 The results for scenarios 1 – 3 are illustrated in sections 4.1, 4.2, and 4.3, respectively.

256 3.6 Detrending of results for long term transients

257 Model simulations were conducted for 1,000 years using 20 years [March-2000 – Feb-2020] of observations in vegetation
258 cover, and precipitation and were repeated 50 times for a total simulation duration of 1000 years. Simulations presented here
259 were conducted on the present-day topography to allow for the application of observed time series of precipitation and
260 vegetation change in different ecosystems and study areas. This choice of setting comes with the compromise that the erosional
261 parameters (e.g., diffusivity, erodibility, etc.) used in the model are likely not the same as those that led to the present-day
262 catchment topography. As a result, a long-term transient in erosion rates is expected as the model tries to reach an equilibrium
263 with assumed erosional parameters. To correct for any long-term transients in erosion influencing our interpretations, we
264 conducted a linear detrending of the results to remove any long-term variations. Hence, the detrended model results for the last
265 20 years were analyzed and discussed in sections 4 and 5.

266 4 Results

267 In the following sections, we focus our analysis on the mean catchment erosion rates over seasonal (3 months) time scales (see
268 Table. 1). In all scenarios, the rock uplift rate was kept constant at 0.05 mm yr^{-1} following the approach of Sharma et al. (2021).
269 For simple representation, the results of the last five years of the last cycle of transient simulations starting from Autumn-2015
270 to Summer-2019 are displayed in Fig. 4, 6, and 8 (after detrending, see section 3.6). The results for the entire time series
271 (Autumn-2000 – Summer-2019) are available in the supplement (Fig. 1 – 3). The precipitation and erosion rates are shown
272 with the units [mm season^{-1}].

273 4.1 Scenario 1: Influence of constant precipitation and seasonal variations in vegetation cover on erosion rates

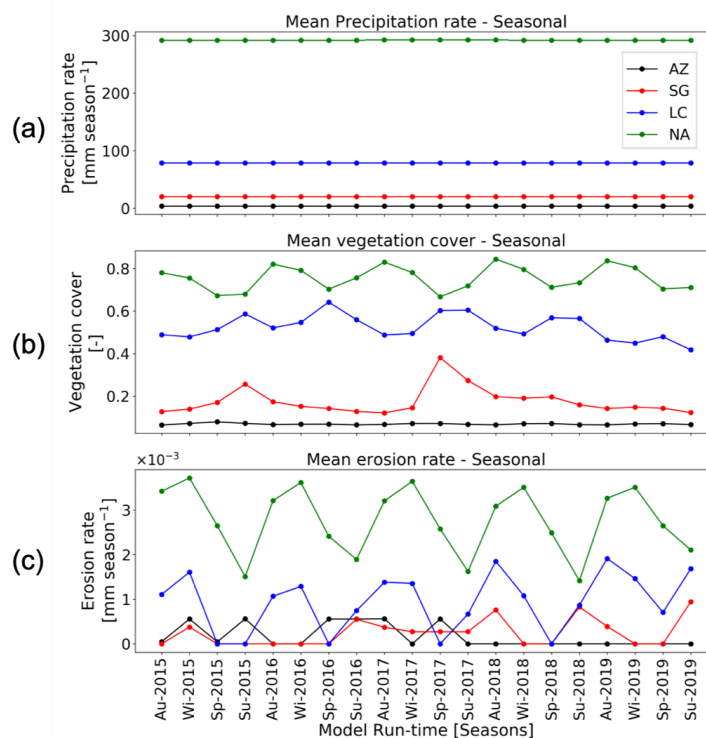
274 In scenario 1, vegetation cover (MODIS NDVI from March 2000 to February 2020) fluctuates seasonally (Fig. 4b), and
275 precipitation rates are kept constant at the seasonal mean (i.e., MAP divided by the number of seasons in a year) during the
276 entire time-series (Fig. 4a) (Ziese et al., 2020). The range of seasonal vegetation cover variations (and mean seasonal
277 precipitation rates) are observed as $0.06 - 0.08 [-]$ ($3.92 \text{ mm season}^{-1}$), $0.1 - 0.4 [-]$ ($20.16 \text{ mm season}^{-1}$), $0.35 - 0.65 [-]$ (79
278 mm season^{-1}), and $0.5 - 0.85 [-]$ ($292 \text{ mm season}^{-1}$) for the Pan de Azúcar, Santa Gracia, La Campana and Nahuelbuta study
279 areas (Fig. 1), respectively.

280 The predicted mean catchment seasonal erosion rates range between $0 - 6 \times 10^{-4} \text{ mm season}^{-1}$, $0 - 9.4 \times 10^{-4} \text{ mm season}^{-1}$,
281 $0 - 2.3 \times 10^{-3} \text{ mm season}^{-1}$, and $1.2 \times 10^{-3} - 4 \times 10^{-3} \text{ mm season}^{-1}$ in Pan de Azúcar, Santa Gracia, La Campana, and
282 Nahuelbuta, respectively (Fig. 4c). The mean catchment seasonal erosion rates have an inverse linear relationship with seasonal
283 vegetation cover for arid, semi-arid, and Mediterranean settings (Fig. 5). However, this relationship is positive in the humid-
284 temperate setting, i.e., erosion increases with an increase in vegetation cover with a relatively lower gradient (3×10^{-3}).

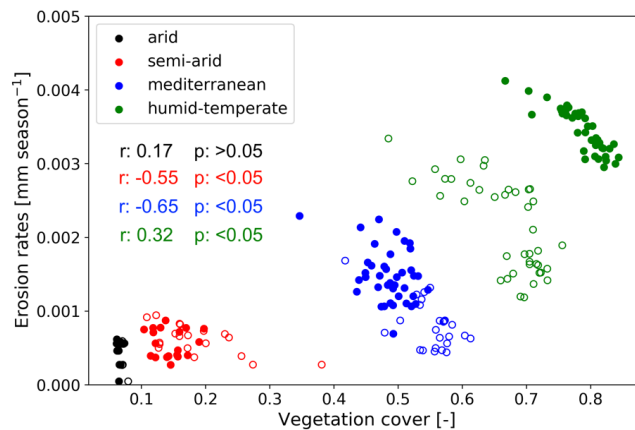
285 The maximum gradient between vegetation cover and erosion rates is observed in the Mediterranean region (La Campana,
286 gradient: -6×10^{-3}). The slopes in the vegetation cover – erosion rate relationship (Fig. 5) represent the sensitivity of each
287 catchment to changes in seasonal vegetation cover, which indicates that the Mediterranean region (La Campana) is ~ 4.5 times
288 more sensitive than the semi-arid region (Santa Gracia). Due to very low precipitation in the arid region (Pan de Azúcar), no
289 significant range in erosion rates is observed (e.g., Pearson $r: 0.17$; $p: >0.05$). The results (Fig. 4 and 5) suggest a high sensitivity
290 in erosion in the Mediterranean setting to changes in seasonal vegetation cover (i.e., erosion rates decrease with an increase in



291 vegetation cover). The erosion rates are low (e.g., <0.005 mm season $^{-1}$) due to low mean precipitation rates subjected to
 292 infiltration and evapotranspiration.



293
 294 **Figure 4. Results of simulations with constant seasonal precipitation and variable vegetation over last 5 years (Autumn-**
 295 **2015 – Summer-2019) of last cycle of transient-state model run representing: (a) mean catchment seasonal precipitation**
 296 **rates [mm season $^{-1}$], (b) mean catchment seasonal vegetation cover [-], and (c) mean catchment seasonal erosion rates**
 297 **[mm season $^{-1}$].**

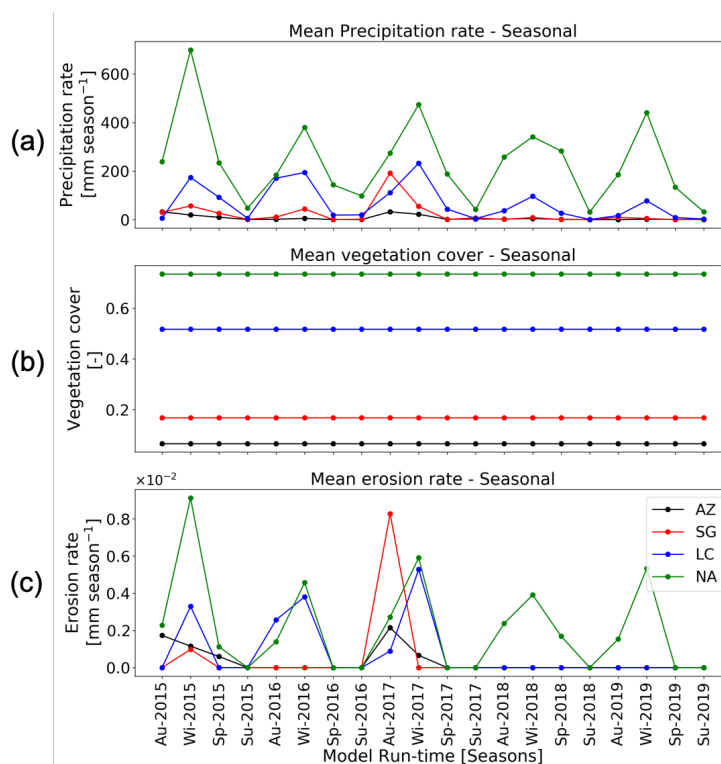


298
 299 **Figure 5. Correlation of vegetation cover [-] and erosion rates [mm season $^{-1}$] obtained from simulations with constant**
 300 **seasonal precipitation and variable vegetation over the last cycle of the transient state model run (Autumn-2000 –**
 301 **Summer-2019). Hollow circles: dry season; filled circles: wet season. Each individual circle represents one predicted**
 302 **season within the timeseries.**



303 **4.2 Scenario 2: Influence of seasonal variations in precipitation and constant vegetation cover on erosion rates**

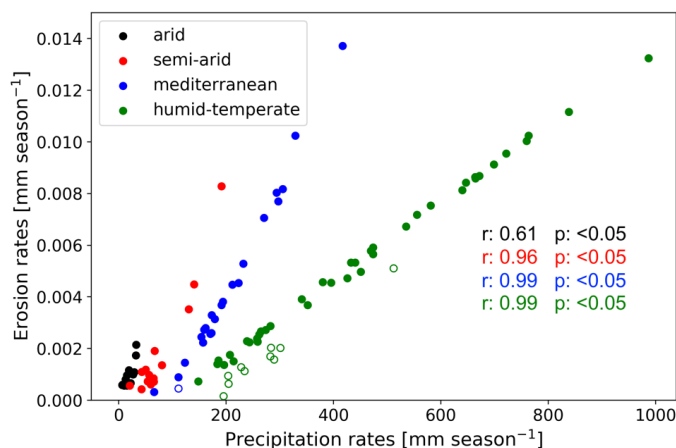
304 In scenario 2, vegetation cover (MODIS NDVI from Mar-2000 – Feb-2020) is kept constant at the mean seasonal vegetation
 305 cover (Fig. 6b) and precipitation rates vary seasonally (Mar-2000 – Feb-2020) (Fig. 6a). The range of seasonal precipitation
 306 rate variations are observed in the range of 0 – 32.42 mm season⁻¹, 0 – 191.66 mm season⁻¹, 0.03 – 417 mm season⁻¹, and 26 –
 307 987 mm season⁻¹ for Pan de Azúcar, Santa Gracia, La Campana and Nahuelbuta, respectively.



308
 309 **Figure 6. Results of simulations with variable seasonal precipitation and constant vegetation over last 5 years (Autumn-**
 310 **2015 – Summer-2019) of last cycle of transient-state model run representing: (a) mean catchment seasonal precipitation**
 311 **rates [mm season⁻¹], (b) mean catchment seasonal vegetation cover [-], and (c) mean catchment seasonal erosion rates**
 312 **[mm season⁻¹].**

313 The simulated mean catchment seasonal erosion rates are observed in the range of 0 – 2 × 10⁻³ mm season⁻¹, 0 – 8.3 × 10⁻³
 314 mm season⁻¹, 0 – 1.37 × 10⁻² mm season⁻¹, and 0 – 1.3 × 10⁻² mm season⁻¹ in Pan de Azúcar, Santa Gracia, La Campana,
 315 and Nahuelbuta, respectively (Fig. 6c). The mean catchment seasonal erosion rates are positively correlated with seasonal
 316 precipitation rates (Fig. 7), with a maximum gradient in the arid region (AZ, gradient: ~1.3 × 10⁻⁴).

317 The gradients in the precipitation – erosion rate relationship (Fig. 7) indicate the sensitivity of each catchment to changes in
 318 seasonal precipitation rates, such that that the arid region (AZ) is ~2.7, ~3.2, and ~8 times more sensitive than semi-arid (SG),
 319 Mediterranean (LC) and humid-temperate region (NA), respectively. The results (Fig. 6 and 7) suggest a high sensitivity of
 320 erosion in the arid and semi-arid settings to changes in seasonal precipitation rates (i.e., erosion increases at relatively higher
 321 rates with an increase in precipitation). The erosion rates are higher than in scenario 1 (e.g., 0 – 0.014 mm season⁻¹) due to
 322 higher precipitation rates in scenario 2.



323

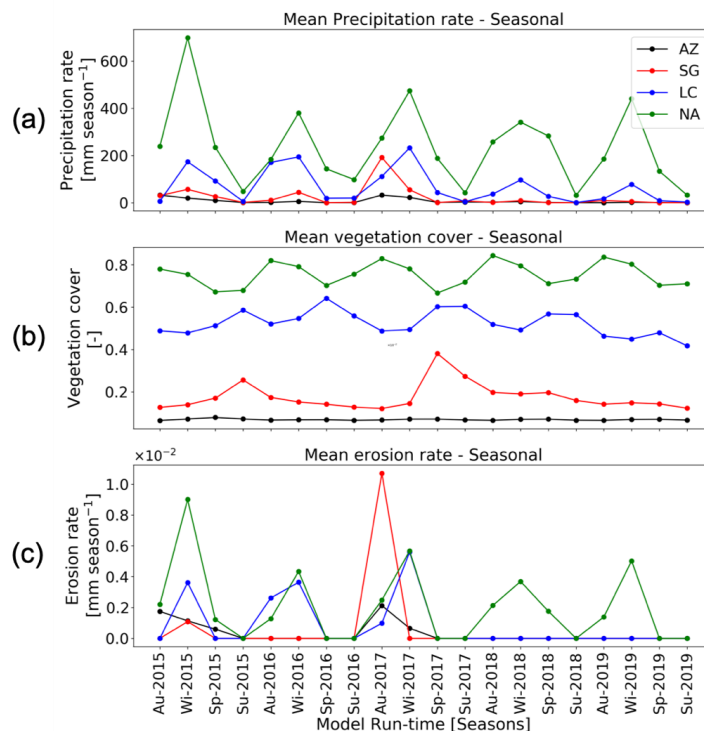
324 **Figure 7. Correlation of precipitation rates [mm season⁻¹] and erosion rates [mm season⁻¹] obtained from simulations**
325 **with variable seasonal precipitation and constant vegetation over the last cycle of the transient state model run**
326 **(Autumn-2000 – Summer-2019). Hollow circles: dry season; filled circles: wet season. Each individual circle represents**
327 **one predicted season within the timeseries.**

328 4.3 Scenario 3: Influence of coupled seasonal variations in both precipitation and vegetation cover on erosion rates

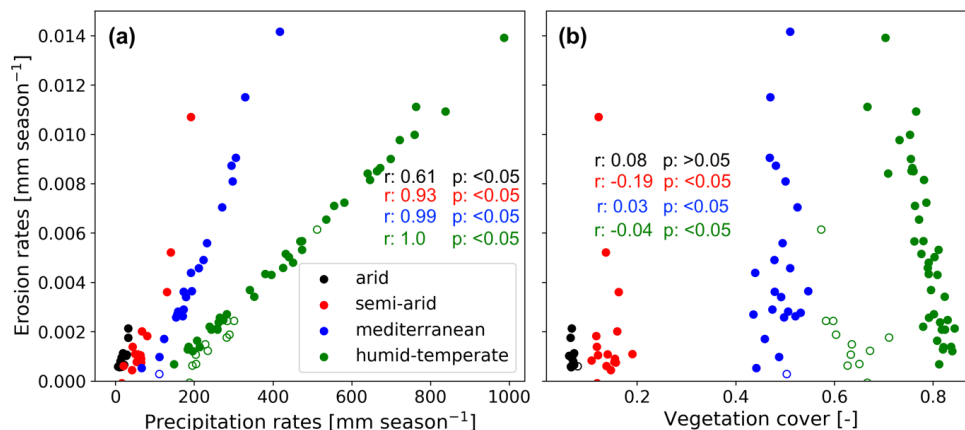
329 In this scenario, coupled variations in seasonal vegetation cover (MODIS NDVI from Mar-2000 – Feb-2020) (Fig. 8b) and
330 precipitation rates are presented for the years 2000 - 2019 (Fig. 8a). The range of seasonal precipitation rates (and seasonal
331 vegetation cover, V) variations are 0 – 32.42 mm season⁻¹ (V= 0.06 – 0.08 [-]), 0 – 191.66 mm season⁻¹ (0.1 – 0.38 [-]), 0.03
332 – 417 mm season⁻¹ (0.35 – 0.65 [-]), and 26 – 987 mm season⁻¹ (0.5 – 0.85 [-]) for Pan de Azúcar, Santa Gracia, La Campana
333 and Nahuelbuta, respectively.

334 The mean catchment seasonal erosion rates are observed in the range of 0 – 2 × 10⁻³ mm season⁻¹, 0 – 1 × 10⁻² mm season⁻¹,
335 0 – 1.4 × 10⁻² mm season⁻¹, and 0 – 1.4 × 10⁻² mm season⁻¹ in Pan de Azúcar, Santa Gracia, La Campana, and
336 Nahuelbuta, respectively (Fig. 8c). Similar to scenario 2, mean catchment seasonal erosion rates are observed to be positively
337 correlated with seasonal precipitation rates (Fig. 9), with a maximum gradient in an arid region (AZ, gradient: ~1.3 × 10⁻⁴).
338 The slopes in the precipitation – erosion rate relationship (Fig. 9) represent the sensitivity of each catchment to coupled
339 variations in seasonal precipitation rates and vegetation cover. The results (Fig. 8 and 9) indicate that the arid region (AZ) is
340 ~2.3, ~3, and ~8 times more sensitive than the semi-arid (SG), Mediterranean (LC), and humid-temperate region (NA),
341 respectively. The similarity in results obtained from scenarios 2 and 3 suggest the first-order control of seasonal precipitation
342 changes on erosion rates (e.g., Pearson r > 0.6 for arid setting, Fig. 9a), with less significance to changing vegetation cover
343 (Pearson r < -0.19 for semi-arid setting, Fig. 9b).

344



345
 346 **Figure 8.** Results of simulations with coupled variations in seasonal precipitation and vegetation over the last five years
 347 (Autumn-2015 – Summer-2019) of the last cycle of transient-state model run representing: (a) mean catchment seasonal
 348 precipitation rates [mm season⁻¹], (b) mean catchment seasonal vegetation cover [-], and (c) mean catchment seasonal
 349 erosion rates [mm season⁻¹].



350
 351 **Figure 9.** Correlation between (a) precipitation rates [mm season⁻¹] and (b) vegetation cover and erosion rates [mm
 352 season⁻¹] obtained from simulations with coupled variations in seasonal precipitation and vegetation over the last cycle
 353 of the transient simulation (Autumn-2000 – Summer-2019). Hollow circles: dry season; filled circles: wet season. Each
 354 individual circle represents one predicted season within the timeseries.

355
 356



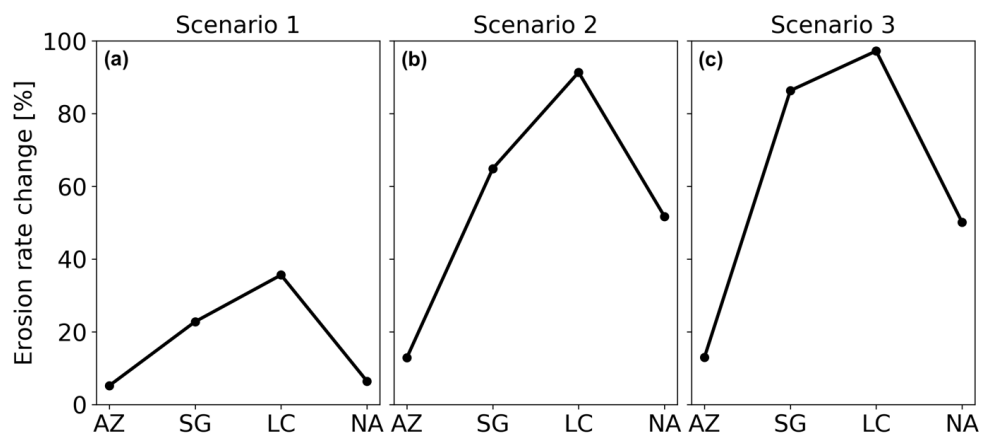
357 5 Discussion

358 This section discusses the relationship between variations in seasonal precipitation and vegetation cover with erosion rates
359 (section 5.1). This is followed by a discussion of the effect of variable vegetation and precipitation rates on seasonal erosion
360 rates (section 5.2). Following this, we present the synthesis of catchment scale erosion rates variability over wet and dry
361 seasons (section 5.3). Finally, we compare our results with previously published studies (section 5.4) and discuss model
362 limitations (section 5.5).

363 5.1 Synthesis of the amplitude of change in erosion rates for model scenarios 1-3

364 The amplitude of change of mean catchment erosion rates [in percentage] varies at a seasonal scale (Fig. 10) between the study
365 areas. The amplitude of change in erosion rates to their respective mean values was estimated (Fig. 10) using the coefficient
366 of variation in percent (standard deviation divided by the mean of a dataset). The coefficient of variation is a statistical tool to
367 compare multiple variables free from scale effects, i.e., it is a dimensionless quantity (Brown, 1998). This comparison
368 represents the sensitivity of each catchment to changing seasonal weather for all three model scenarios (section 4.1 – 4.3).

369 In scenario 1, with seasonal variations in vegetation cover and constant seasonal precipitation (Fig. 10a), the amplitude of
370 change in erosion rates ranges between 6.5% in the humid-temperate setting and 36% in Mediterranean setting. The above
371 results support the findings of Zhang et al. (2019), which observed 20-30% of the total change in sediment yield with constant
372 precipitation and variable vegetation cover. The above study used the soil and water assessment tool (SWAT) based on NDVI
373 and climate parameters. In addition, a 5.5% change in amplitude in erosion rates is observed in the arid setting (Fig. 10a).
374 However, due to the weak correlation between vegetation cover and erosion rates (i.e., Pearson r : 0.17 and $p > 0.05$, Fig. 5) and
375 negligible vegetation cover ($V < 0.1$), it is unclear if these changes in erosion rates are due to changes in vegetation cover
376 alone.



377
378 **Figure 10. The amplitude of change in seasonal erosion rates (relative to their respective means) in (a) scenario 1: with**
379 **variable vegetation cover and constant precipitation rates, (b) scenario 2: with constant vegetation cover and variable**
380 **precipitation rates, and (c) scenario 3: with coupled variations in vegetation cover and precipitation rates.**

381 In scenario 2, with constant vegetation cover and variable precipitation rates (Fig. 10b), the amplitude of change in erosion
382 rates ranges from 13% in the arid setting (AZ) to 52%, 65%, and 91% in humid-temperate (NA), semi-arid (SG) and
383 Mediterranean (LC) settings, respectively. A similar trend is observed in scenario 3 with coupled variations in vegetation cover
384 and precipitation rates (Fig. 10c), with the amplitude of change in erosion rates between 13% in the arid setting up to 50%,
385 86%, and 97% in the humid-temperate, semi-arid and Mediterranean settings, respectively. The magnitude of erosion rate
386 changes is amplified in scenario 3, especially in the semi-arid setting (e.g., ~21% increase in the amplitude of change from

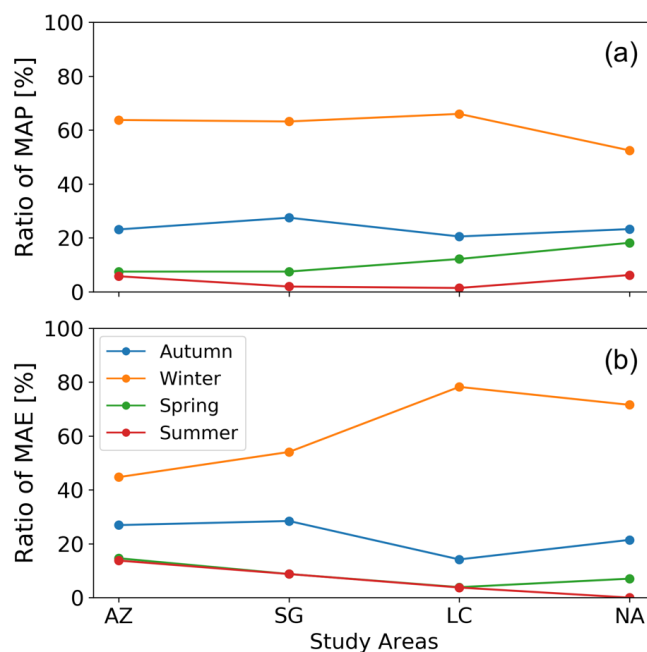


387 scenario 2 to scenario 3). This amplification could be owed to the 35% change in vegetation cover in the semi-arid setting (Fig.
388 8). Overall, these observations indicate a high sensitivity of erosion in semi-arid and Mediterranean environments compared
389 to arid and humid-temperate settings.

390 The pattern of erosion rate changes in scenarios 1-3 implies a predominant control of precipitation variations (rather than
391 vegetation cover change) on catchment erosion rates at a seasonal scale. This interpretation is consistent with previous
392 observational studies. For example, a plot-scale study by Gabarrón-Galeote et al. (2013) in the Mediterranean environment in
393 Belgium concluded that rainfall intensity was the main factor in determining the observed seasonal soil hydrological and
394 erosive response. Another field study by Suescún et al. (2017) in the Columbian Andes highlighted the significant influence
395 of precipitation seasonality (over vegetation cover seasonality) on runoff and erosion rates. An observational catchment-scale
396 study in the semi-arid Chinese Loess Plateau by Wei et al. (2015) indicated that intra-annual precipitation variations were a
397 significant contributor to monthly runoff and sediment yield variations.

398 5.2 Synthesis of catchment erosion rates over wet and dry seasons

399 In this section, we discuss the ratio of MAP (Fig. 11a) and mean annual erosion (MAE) (Fig. 11b) during different seasons
400 (i.e., autumn – summer) in a year, averaged over the entire time series (2000 – 2019). This analysis is performed for the
401 simulation results of scenario 3 for different climate and ecological settings (i.e., arid to humid-temperate). We do this
402 specifically with scenario 3 results to capture the trends in erosion rates with coupled variations in model input (i.e.,
403 precipitation and vegetation cover).



404
405 **Figure 11.** The ratio of model variables to annual means during all the seasons in a year for simulation results from
406 scenario 3 (coupled seasonal variations in precipitation and vegetation cover). The plots correspond to (a) ratio of MAP
407 per season [%] and (b) ratio of MAE per season [%] of the mean values averaged over the last 20 years of the
408 simulations (2000 - 2019). Each point represents the ratio for each ecological setting i.e., arid (Pan de Azúcar, AZ),
409 semi-arid (Santa Gracia, SG), Mediterranean (La Campana, LC), and humid-temperate settings (Nahuelbuta, NA).



410 The values for the ratio of MAP during different seasons (Fig. 11a) depicts winter (June-August) and summer (December-
411 February) as the wettest and driest seasons of the year, respectively. For example, all study areas receive >50% and <6% of
412 MAP during winters and summers. The same is reflected in Fig. 11b with 45%, 55%, 78%, and 71% of MAE in the arid, semi-
413 arid, Mediterranean, and humid-temperate settings, respectively, during winters. On the contrary, during summers the share of
414 MAE decreases from 14% in the arid setting to 1% in the humid-temperate setting. The Autumn (March-May) receives lower
415 precipitation amounts that range from 20–30% of MAP in the study areas. Arid and semi-arid settings experience a relatively
416 higher share of MAE (e.g., ~30%) than the Mediterranean and humid temperate settings (e.g., ~15-20%). The Spring season
417 experiences relatively higher erosion rates despite a smaller share of MAP in arid and semi-arid settings. For example, the arid
418 and semi-arid settings experience 10-14% of the MAE for ~7% of MAP. At the same time, the Mediterranean and humid-
419 temperate settings experience 5-7% of MAE for ~12-18% of MAP during Spring. Overall, we find that arid and semi-arid
420 settings experience <15% and ~50% of MAE during the wet (winter) and dry (summer) seasons. The above relationship is
421 amplified for the Mediterranean and humid-temperate settings with <5% and >70% of MAE occurring during wet and dry
422 seasons, respectively. The latter is in agreement with an observational study by Mosaffaie et al., (2015) in a Mediterranean
423 catchment in Iran. More specifically, Mosaffaie et al., (2015) used field observations from 2012-2013 to conclude that
424 maximum erosion rates (>70%) are observed during the wet season, which decreases in the dry season (<10%).

425 5.3 Comparison to previous studies

426 In this section, we relate the broad findings of this study to the previously published observational studies. In an observational
427 study in an agrarian drainage basin in the Belgian Loam Belt, Steegen et al., (2000) evaluated sediment transport over various
428 time scales (including seasonal). They observed lower sediment fluxes during the seasons with high vegetation cover. In
429 addition, an observational study by Zheng (2006) investigated the effect of vegetation changes on soil erosion in the Loess
430 Plateau, China, and concluded that soil erosion was significantly reduced (up to ~50%) after vegetation restoration. Another
431 observational study in semi-arid grasslands in Loess Plateau, China, by Hou et al., (2020) highlighted a considerable reduction
432 in erosion rates due to the development of richness and evenness of the plant community in the early to the mid wet season.
433 Our results from scenario 1 (seasonal variations in vegetation cover with constant precipitation rates) support the findings of
434 the above studies whereby a negative correlation (Pearson r : ~-0.6 and p <0.05) was found between vegetation cover and
435 erosion rates for the semi-arid and Mediterranean settings. More specifically, we found erosion rates decrease with an increase
436 in vegetation cover in Santa Gracia (semi-arid) and La Campana (Mediterranean) (see Fig. 5). However, a positive correlation
437 (Pearson r : ~0.3 and p <0.05) is observed in the humid-temperate setting from dry season to wet season (see Fig. 5).

438 A catchment-scale observational study in Baspa Valley, NW Himalayas (Wulf et al., 2010), analyzed seasonal precipitation
439 gradients and their impact on fluvial erosion using weather station observations (1998 – 2007). The study observed a positive
440 correlation between precipitation and sediment yield variability, demonstrating the summer monsoon's first-order control on
441 erosion processes. An observational study by Wei et al., (2015) in Loess Plateau, China, evaluated erosion and sediment
442 transport under various vegetation types and precipitation variations. They found that significant changes in vegetation cover
443 might contribute to long-term soil dynamics. However, seasonal variations in runoff and sediment yield were mainly influenced
444 by rainfall seasonality. In comparison to the results of this study, we find the similarity in the patterns of erosion rates in
445 scenario 2 (variable precipitation and constant vegetation cover) and scenario 3 (coupled variations in precipitation and
446 vegetation) are consistent with the findings of Wei et al., (2015). For example, the amplitude of change in erosion rates (Fig.
447 10) in scenarios 2 and 3 differ by 0%, 6%, and -2% in the arid, Mediterranean, and humid-temperate settings, respectively.
448 However, this difference is enhanced in the semi-arid region (i.e., ~23%) due to a relatively high degree of variation (~25%)
449 in seasonal vegetation cover change.

450 Finally, an observational study in the Columbian Andes by Suescún et al., (2017) assessed the impact of seasonality on
451 vegetation cover and precipitation and found higher erosion rates in regions with steeper slopes. Another study by Chakrapani



452 (2005) emphasized the direct impact of local relief and channel slope on sediment yield in natural rivers. The broad findings
453 of the above studies agree with our results from scenarios 1-3, as we find higher erosion rates in the Mediterranean and humid-
454 temperate regions with steeper topography (mean slope ~20 deg), which encounter high seasonality (and intensity) in
455 precipitation.

456 **5.4 Model Limitations**

457 The model setup used in this study was designed to quantify the sensitivity of erosion rates in different climate and ecological
458 settings with variations in precipitation rates and vegetation cover at seasonal scales. We represent the degree of variations in
459 erosion rates in terms of change amplitude (with respect to the mean) for different model scenarios (see sections 4.1 – 4.3).
460 This study was intended to introduce temporal downscaling (from millennial to seasonal time scales) to the approach of
461 previous similar modeling studies (e.g., Schmid et al., 2018; Sharma et al., 2021).

462 Our modeling approach used several simplifying assumptions that warrant discussion and potential investigation in future
463 studies. For example, model results presented here successfully capture the major surface processes, including vegetation-
464 dependent erosion and infiltration, sediment transport, and surface runoff. However, groundwater flow is not considered in
465 the current study, and how the reentry of groundwater into streams over seasonal scales would influence downstream erosion.
466 The reason is that groundwater flow modeling includes a high amount of heterogeneity and anisotropy and requires much finer
467 grid sizes (<1m) and smaller time steps (in seconds to hours). Thus, due to the large grid-cell size (90 m), timescales (monthly),
468 and high uncertainty in subsurface hydrologic parameters we were unable to evaluate the effects of groundwater flow on our
469 results. Furthermore, this study assumed uniform lithological and hydrological parameters (e.g., vertical hydraulic
470 conductivity, initial soil moisture, evapotranspiration, erodibility, etc.) over the entire catchment. As said earlier, these
471 properties are subjected to a high level of uncertainty and heterogeneity, the best fitting parameters, based on previously
472 published literature (e.g., Schaller et al., 2018; Bernhard et al., 2018; Schmid et al., 2018; Sharma et al., 2021) are used for the
473 model simulations. However, the heterogeneity in vegetation cover and related soil-water infiltration per grid cell is used in
474 this study. For the heterogeneity in vegetation cover, we use MODIS-derived NDVI as a proxy of vegetation cover. According
475 to Garatuza-Payán et al. (2005), NDVI is assumed as an effective tool for estimating seasonal changes in vegetation cover
476 density. However, the spatial resolution (250 m) of the NDVI dataset is lower than that of the SRTM DEM (90 m) used in the
477 study. Nevertheless, the difference in spatial resolution of vegetation cover and topography might introduce ambiguity in the
478 model results.

479 A final limitation stems from several generalized model parameters (e.g., rock uplift rate, erodibility, diffusivity, etc.) applied
480 to the SRTM DEM (as initial topography). We did this to capture the effects of seasonality in precipitation and vegetation
481 cover in modern times (2000 - 2019). However, the current topography might not have evolved with the same tectonic and
482 lithological parameters. To address this limitation, we simulated the model for 50 iterations and detrended the model results
483 to remove those transient effects (see section 3.6). This limitation can be handled in future studies by parameterizing the model
484 to the current topography using stochastic (e.g., Bayesian) techniques (e.g., Stephenson et al., 2006; Avdeev et al., 2011). As
485 this study was aimed to capture the control of seasonal precipitation and (or) vegetation changes on the relative variability of
486 erosion rates, the above limitation may not pose a problem in the model results.

487 **6 Summary and Conclusions**

488 In this study, we applied a landscape evolution model to quantify the impact of seasonal variations in precipitation and
489 vegetation on catchment averaged erosion rates. We performed this in regions with varied climate and ecology including: arid,
490 semi-arid, Mediterranean, and humid-temperate settings. Three sets of simulations were designed to model erosion rates for
491 (a) scenario 1: constant precipitation and variable vegetation cover, (b) scenario 2: variable precipitation and constant



492 vegetation cover, and (c) scenario 3: coupled variations in precipitation and vegetation cover. The main conclusions derived
493 from this study are as follows:

- 494 1. Scenario 1, with variable vegetation cover and constant precipitation (Fig. 4), resulted in small variations in seasonal
495 erosion rates ($<0.02 \text{ mm yr}^{-1}$) in comparison to the other scenarios. The amplitude of change in seasonal erosion rates
496 (relative to the mean) is the smallest in humid-temperate setting and maximum in the Mediterranean setting (Fig.
497 10a). For example, it ranges from 6.5% in humid-temperate setting (Nahuelbuta) to 23% and 36% in semi-arid (Santa
498 Gracia) and Mediterranean settings (La Campana), respectively.
- 499 2. Scenario 2, with constant vegetation cover and variable precipitation (Fig. 6), results in relatively higher seasonal
500 erosion rates ($<0.06 \text{ mm yr}^{-1}$) in comparison to scenario 1. The amplitude of change in seasonal erosion rates (relative
501 to the mean) is smallest in the arid setting and the largest in the Mediterranean setting (Fig. 10b). For example, it
502 ranges from 13% in the arid setting (Pan de Azúcar) to 52%, 65%, and 91% in humid-temperate (Nahuelbuta), semi-
503 arid (Santa Gracia), and Mediterranean settings (La Campana), respectively.
- 504 3. Scenario 3, with coupled variations in vegetation cover and precipitation (Fig. 8), results in similar seasonal erosion
505 rates ($<0.06 \text{ mm yr}^{-1}$) to scenario 2. Similarly, the amplitude of change in seasonal erosion rates (relative to the mean)
506 is the smallest in the arid setting and the largest in the Mediterranean setting (Fig. 10c). For example, it ranges from
507 13% in the arid setting (Pan de Azúcar) to 50%, 86%, and 97% in humid-temperate (Nahuelbuta), semi-arid (Santa
508 Gracia), and Mediterranean settings (La Campana), respectively. A significant increase (from scenario 2) in variation
509 in erosion rates ($\sim 21\%$) is owed to the $\sim 25\%$ variation in vegetation cover in semi-arid settings.
- 510 4. All study areas experience maximum and minimum erosion during wet and dry seasons, respectively (Fig. 11b).
511 However, the difference (in maximum and minimum) is amplified from the arid ($\sim 30\%$) to the Mediterranean and
512 humid-temperate settings ($\sim 70\text{--}75\%$). This is owed to the range of amplitude of precipitation rate change (Fig. 7)
513 increasing from the arid (e.g., $\sim 9 \text{ mm}$) to humid-temperate settings (e.g., $\sim 543 \text{ mm}$) in wet and dry seasons.

514 Finally, this study was motivated by testing the hypotheses that (1) if precipitation variations primarily influence seasonal
515 erosion, then the influence of seasonal vegetation cover changes would be less significant, and (2) catchment erosion in drier
516 settings is more sensitive to seasonality in precipitation and vegetation, than wetter settings. With respect to hypothesis 1, we
517 found that seasonal precipitation variations primarily drive catchment erosion and the effects of vegetation cover variations
518 are secondary. Results presented here (Fig. 10b) support this interpretation with significantly high amplitude of change in
519 erosion rates (with respect to means) ranging from 13 to 91% for scenario with constant vegetation cover and seasonal
520 precipitation variations. However, the effect of seasonal vegetation cover changes is also significant (Fig. 10a) ranging between
521 5 – 36%. Hence, the first hypothesis is partially confirmed. Concerning hypothesis 2, we found that seasonal changes in
522 catchment erosion are more pronounced in semi-arid and Mediterranean settings and less in arid and humid temperate settings.
523 This interpretation is supported by Fig. 10c, with significantly high amplitude of change in catchment erosion in semi-arid
524 ($\sim 86\%$) and Mediterranean ($\sim 97\%$) settings with relatively lower changes in humid temperate ($\sim 50\%$) and arid ($\sim 13\%$) settings,
525 partially confirming the hypothesis.

526

527

528

529

530



531 **Appendix**

532 **Table A1. Input parameters with corresponding units for the landscape evolution model**

Model Parameters	Values
Grid spacing (dx)	90 m
Model runtime (totalT)	1000 years (2000 – 2019 repeated over 50 times)
time-step (dt)	1 season (3 months)
Rock uplift rate (U) ¹	1.25 x 10 ⁻⁵ [m season ⁻¹] (or 0.05 [mm a ⁻¹])
Initial sediment thickness (H_initial) ²	20 (AZ), 0.45 (SG), 0.6 (LC), 0.7 (NA) [cm]
Bedrock erodibility (Kr) ¹	2 x 10 ⁻⁹ [m ⁻¹]
Sediment erodibility (Ks) ¹	2 x 10 ⁻⁸ [m ⁻¹]
Reach scale bedrock roughness (H*) ¹	1 [m]
Porosity (φ) ¹	0.2 [-]
Fraction of fine sediments (Ff) ¹	0.2 [-]
Effective terminal settling velocity (Vs) ¹	2.5 [m season ⁻¹]
m, n ¹	0.6, 1 [-]
Bedrock erosion threshold stream power (ω_cr) ¹	1.25 x 10 ⁻⁵ [m season ⁻¹]
Sed. entr. threshold stream power (ω_cs) ¹	1.25 x 10 ⁻⁶ [m season ⁻¹]
Bare soil diffusivity (K _b) ¹	2.5 x 10 ⁻⁴ [m ² season ⁻¹]
Exponential decay coefficient (α) ¹	0.3 [-]
Critical channel formation area (A _{crit}) ³	1 x 10 ⁶ [m ²]
Reference vegetation cover (V _r) ³	1 (100%)
Manning's number for bare soil (n _b) ³	0.01 [-]
Manning's number for ref. vegetation (n _v) ³	0.6 [-]
Sacling factor for vegetation influence (w) ³	1 [-]
Soil bulk density (B) ⁴	1300 (AZ), 1500 (SG), 1300 (LC), 800 (NA) [kg m ⁻³]
Soil type ⁴	sandy loam (AZ, SG, LC); sandy clay loam (NA)
Initial soil moisture (s) ⁴	0.058 (AZ), 0.02 (SG), 0.053 (LC), 0.15 (NA) [m ³ m ⁻³]

533
 534 ¹ Sharma et al. (2021), ² Schaller et al. (2018), ³ Schmid et al. (2018), ⁴ Bernhard et al. (2018).

535 **Code and data availability**

536 The code and data used in this study are freely available upon request.

537 **Author contributions**

538 HS and TAE designed the initial model setup and simulation programs. HS and TAE conducted model modifications,
 539 simulation runs, and analysis. HS prepared the paper with contributions from TAE.

540 **Competing interests**

541 The authors declare that they have no conflict of interest.

542 **Acknowledgments**

543 Hemanti Sharma and Todd A. Ehlers acknowledge support from the Open Access Publishing Fund of the University of
 544 Tübingen. We also acknowledge support from the Research Training Group 1829 Integrated Hydrosystem Modelling, funded
 545 by the German Research Foundation (DFG). In addition, Todd A. Ehlers acknowledges support from the German priority
 546 research program “EarthShape: Earth Surface Shaping by Biota” (SPP-1803; EH329/14-2). We thank xxx and yyy for their
 547 constructive reviews.



548 **References**

- 549 Avdeev, B., Niemi, N. A., and Clark, M. K.: Doing more with less: Bayesian estimation of erosion models with detrital
550 thermochronometric data, *Earth Planet. Sci. Lett.*, 305, 385–395, <https://doi.org/10.1016/j.epsl.2011.03.020>, 2011.
- 551 Barnhart, K. R., Glade, R. C., Shobe, C. M., and Tucker, G. E.: Terrainbento 1.0: a Python package for multi-model analysis
552 in long-term drainage basin evolution, *Geosci. Model Dev.*, 12, 1267–1297, <https://doi.org/10.5194/gmd-12-1267-2019>, 2019.
- 553 Beaudoin, H., Rodell, M., and NASA/GSFC/HSL: GLDAS Noah Land Surface Model L4 monthly 0.25 x 0.25 degree,
554 Version 2.1, <https://doi.org/10.5067/SXAVCZFAQLNO>, 2020.
- 555 Bernhard, N., Moskwa, L.-M., Schmidt, K., Oeser, R. A., Aburto, F., Bader, M. Y., Baumann, K., von Blanckenburg, F., Boy,
556 J., van den Brink, L., Brucker, E., Büdel, B., Canessa, R., Dippold, M. A., Ehlers, T. A., Fuentes, J. P., Godoy, R., Jung, P.,
557 Karsten, U., Köster, M., Kuzyakov, Y., Leinweber, P., Neidhardt, H., Matus, F., Mueller, C. W., Oelmann, Y., Oses, R., Osses,
558 P., Paulino, L., Samolov, E., Schaller, M., Schmid, M., Spielvogel, S., Spohn, M., Stock, S., Stroncik, N., Tielbörger, K.,
559 Übernicket, K., Scholten, T., Seguel, O., Wagner, D., and Kühn, P.: Pedogenic and microbial interrelations to regional climate
560 and local topography: New insights from a climate gradient (arid to humid) along the Coastal Cordillera of Chile, *CATENA*,
561 170, 335–355, <https://doi.org/10.1016/j.catena.2018.06.018>, 2018.
- 562 Bookhagen, B., Thiede, R. C., and Strecker, M. R.: Abnormal monsoon years and their control on erosion and sediment flux
563 in the high, arid northwest Himalaya, *Earth Planet. Sci. Lett.*, 231, 131–146, <https://doi.org/10.1016/j.epsl.2004.11.014>, 2005.
- 564 Brown, C. E.: Coefficient of Variation, in: *Applied Multivariate Statistics in Geohydrology and Related Sciences*, Springer,
565 Berlin, Heidelberg, 1998.
- 566 Carretier, S., Tolorza, V., Regard, V., Aguilar, G., Bermúdez, M. A., Martinod, J., Guyot, J.-L., Hérail, G., and Riquelme, R.:
567 Review of erosion dynamics along the major N-S climatic gradient in Chile and perspectives, *Geomorphology*, 300, 45–68,
568 <https://doi.org/10.1016/j.geomorph.2017.10.016>, 2018.
- 569 Cerdà, A.: The influence of aspect and vegetation on seasonal changes in erosion under rainfall simulation on a clay soil in
570 Spain, *Can. J. Soil Sci.*, 78, 321–330, <https://doi.org/10.4141/S97-060>, 1998.
- 571 Chakrapani, G. J.: Factors controlling variations in river sediment loads, *Curr. Sci.*, 88, 569–575, 2005.
- 572 Deal, E., Favre, A. C., and Braun, J.: Rainfall variability in the Himalayan orogen and its relevance to erosion processes:
573 RAINFALL VARIABILITY IN THE HIMALAYAS, *Water Resour. Res.*, 53, 4004–4021,
574 <https://doi.org/10.1002/2016WR020030>, 2017.
- 575 Didan, Kamel: MOD13Q1 MODIS/Terra Vegetation Indices 16-Day L3 Global 250m SIN Grid V006,
576 <https://doi.org/10.5067/MODIS/MOD13Q1.006>, 2015.
- 577 Earth Resources Observation And Science (EROS) Center: Shuttle Radar Topography Mission (SRTM) Void Filled,
578 <https://doi.org/10.5066/F7F76B1X>, 2017.
- 579 Ferreira, V. and Panagopoulos, T.: Seasonality of Soil Erosion Under Mediterranean Conditions at the Alqueva Dam
580 Watershed, *Environ. Manage.*, 54, 67–83, <https://doi.org/10.1007/s00267-014-0281-3>, 2014.
- 581 Gabarrón-Galeote, M. A., Martínez-Murillo, J. F., Quesada, M. A., and Ruiz-Sinoga, J. D.: Seasonal changes in the soil
582 hydrological and erosive response depending on aspect, vegetation type and soil water repellency in different Mediterranean
583 microenvironments, *Solid Earth*, 4, 497–509, <https://doi.org/10.5194/se-4-497-2013>, 2013.
- 584 Gao, P., Li, Z., and Yang, H.: Variable discharges control composite bank erosion in Zoige meandering rivers, *CATENA*, 204,
585 105384, <https://doi.org/10.1016/j.catena.2021.105384>, 2021.
- 586 Garatuza-Payán, J., Sánchez-Andrés, R., Sánchez-Carrillo, S., and Navarro, J. M.: Using remote sensing to investigate erosion
587 rate variability in a semiarid watershed, due to changes in vegetation cover, *IAHS Publ*, 292, 144–151, 2005.
- 588 Glodny, J., Gräfe, K., Echter, H., and Rosenau, M.: Mesozoic to Quaternary continental margin dynamics in South-Central
589 Chile (36–42°S): the apatite and zircon fission track perspective, *Int. J. Earth Sci.*, 97, 1271–1291,
590 <https://doi.org/10.1007/s00531-007-0203-1>, 2008.
- 591 Green, W. H. and Ampt, G. A.: Studies on Soil Physics., *J. Agric. Sci.*, 4, 1–24, <https://doi.org/10.1017/S0021859600001441>,
592 1911.
- 593 Hancock, G. and Lowry, J.: Hillslope erosion measurement—a simple approach to a complex process, *Hydrol. Process.*, 29,
594 4809–4816, 2015.
- 595 Hancock, G. and Lowry, J.: Quantifying the influence of rainfall, vegetation and animals on soil erosion and hillslope
596 connectivity in the monsoonal tropics of northern Australia, *Earth Surf. Process. Landf.*, 46, 2110–2123,
597 <https://doi.org/10.1002/esp.5147>, 2021.
- 598 Herrmann, S. M. and Mohr, K. I.: A Continental-Scale Classification of Rainfall Seasonality Regimes in Africa Based on
599 Gridded Precipitation and Land Surface Temperature Products, *J. Appl. Meteorol. Climatol.*, 50, 2504–2513,
600 <https://doi.org/10.1175/JAMC-D-11-024.1>, 2011.



- 601 Hobley, D. E. J., Adams, J. M., Nudurupati, S. S., Hutton, E. W. H., Gasparini, N. M., Istanbuluoglu, E., and Tucker, G. E.:
602 Creative computing with Landlab: an open-source toolkit for building, coupling, and exploring two-dimensional numerical
603 models of Earth-surface dynamics, *Earth Surf. Dyn.*, 5, 21–46, <https://doi.org/10.5194/esurf-5-21-2017>, 2017.
- 604 Hou, J., Zhu, H., Fu, B., Lu, Y., and Zhou, J.: Functional traits explain seasonal variation effects of plant communities on soil
605 erosion in semiarid grasslands in the Loess Plateau of China, *Catena*, v. 194, 104743–,
606 <https://doi.org/10.1016/j.catena.2020.104743>, 2020.
- 607 Istanbuluoglu, E. and Bras, R. L.: On the dynamics of soil moisture, vegetation, and erosion: Implications of climate variability
608 and change, *Water Resour. Res.*, 42, 2006.
- 609 Johnstone, S. A. and Hilley, G. E.: Lithologic control on the form of soil-mantled hillslopes, *Geology*, 43, 83–86,
610 <https://doi.org/10.1130/G36052.1>, 2014.
- 611 Julien, P. Y., Saghaian, B., and Ogden, F. L.: RASTER-BASED HYDROLOGIC MODELING OF SPATIALLY-VARIED
612 SURFACE RUNOFF1, *JAWRA J. Am. Water Resour. Assoc.*, 31, 523–536, <https://doi.org/10.1111/j.1752-1688.1995.tb04039.x>, 1995.
- 614 Langbein, W. B. and Schumm, S. A.: Yield of sediment in relation to mean annual precipitation, *Eos Trans. Am. Geophys.*
615 *Union*, 39, 1076–1084, <https://doi.org/10.1029/TR039i006p01076>, 1958.
- 616 Leyland, J., Hackney, C. R., Darby, S. E., Parsons, D. R., Best, J. L., Nicholas, A. P., Aalto, R., and Lague, D.: Extreme flood-
617 driven fluvial bank erosion and sediment loads: direct process measurements using integrated Mobile Laser Scanning (MLS)
618 and hydro-acoustic techniques: Direct measurement of flood-driven erosion using MLS and MBES, *Earth Surf. Process.*
619 *Landf.*, 42, 334–346, <https://doi.org/10.1002/esp.4078>, 2016.
- 620 Melnick, D.: Rise of the central Andean coast by earthquakes straddling the Moho, *Nat. Geosci.*, 9, 401–407,
621 <https://doi.org/10.1038/ngeo2683>, 2016.
- 622 Melnick, D., Bookhagen, B., Strecker, M. R., and Echtler, H. P.: Segmentation of megathrust rupture zones from fore-arc
623 deformation patterns over hundreds to millions of years, Arauco peninsula, Chile: EARTHQUAKE SEGMENTATION AT
624 ARAUCO, *J. Geophys. Res. Solid Earth*, 114, <https://doi.org/10.1029/2008JB005788>, 2009.
- 625 Mosaffaie, J., Ekhtesasi, M. R., Dastorani, M. T., Azimzadeh, H. R., and Zare Chahuki, M. A.: Temporal and spatial variations
626 of the water erosion rate, *Arab. J. Geosci.*, 8, 5971–5979, <https://doi.org/10.1007/s12517-014-1628-z>, 2015.
- 627 Oeser, R. A., Stroncik, N., Moskwa, L.-M., Bernhard, N., Schaller, M., Canessa, R., Brink, L. van den, Köster, M., Brucker,
628 E., Stock, S., Fuentes, J. P., Godoy, R., Matus, F. J., Pedraza, R. O., McIntyre, P. O., Paulino, L., Seguel, O., Bader, M. Y.,
629 Boy, J., Dippold, M. A., Ehlers, T. A., Kühn, P., Kuzyakov, Y., Leinweber, P., Scholten, T., Spielvogel, S., Spohn, M.,
630 Übernickel, K., Tielbörger, K., Wagner, D., and Blanckenburg, F. von: Chemistry and microbiology of the Critical Zone along
631 a steep climate and vegetation gradient in the Chilean Coastal Cordillera, *CATENA*, 170, 183–203,
632 <https://doi.org/10.1016/j.catena.2018.06.002>, 2018.
- 633 Rengers, F. K., McGuire, L., Kean, J. W., Staley, D. M., and Hobley, D. E. J.: Model simulations of flood and debris flow
634 timing in steep catchments after wildfire, *Water Resour. Res.*, 52, 6041–6061, <https://doi.org/10.1002/2015WR018176>, 2016.
- 635 Rodell, M., Houser, P. R., Jambor, U., Gottschalk, J., Mitchell, K., Meng, C.-J., Arsenault, K., Cosgrove, B., Radakovich, J.,
636 Bosilovich, M., Entin, J. K., Walker, J. P., Lohmann, D., and Toll, D.: The Global Land Data Assimilation System, *Bull. Am.*
637 *Meteorol. Soc.*, 85, 381–394, <https://doi.org/10.1175/BAMS-85-3-381>, 2004.
- 638 Schaller, M. and Ehlers, T. A.: Comparison of soil production, chemical weathering, and physical erosion rates along a climate
639 and ecological gradient (Chile) to global observations, *Earth Surf. Dyn.*, 10, 131–150, <https://doi.org/10.5194/esurf-10-131-2022>, 2022.
- 641 Schaller, M., Ehlers, T. A., Lang, K. A. H., Schmid, M., and Fuentes-Espoz, J. P.: Addressing the contribution of climate and
642 vegetation cover on hillslope denudation, Chilean Coastal Cordillera (26°–38°S), *Earth Planet. Sci. Lett.*, 489, 111–122,
643 <https://doi.org/10.1016/j.epsl.2018.02.026>, 2018.
- 644 Schaller, M., Dal Bo, I., Ehlers, T. A., Klotzsche, A., Drews, R., Fuentes Espoz, J. P., and van der Kruk, J.: Comparison of
645 regolith physical and chemical characteristics with geophysical data along a climate and ecological gradient, Chilean Coastal
646 Cordillera (26 to 38°S), *SOIL*, 6, 629–647, <https://doi.org/10.5194/soil-6-629-2020>, 2020.
- 647 Schmid, M., Ehlers, T. A., Werner, C., Hickler, T., and Fuentes-Espoz, J.-P.: Effect of changing vegetation and precipitation
648 on denudation – Part 2: Predicted landscape response to transient climate and vegetation cover over millennial to million-year
649 timescales, *Earth Surf. Dyn.*, 6, 859–881, <https://doi.org/10.5194/esurf-6-859-2018>, 2018.
- 650 Sharma, H., Ehlers, T. A., Glotzbach, C., Schmid, M., and Tielbörger, K.: Effect of rock uplift and Milankovitch timescale
651 variations in precipitation and vegetation cover on catchment erosion rates, *Earth Surf. Dyn.*, 9, 1045–1072,
652 <https://doi.org/10.5194/esurf-9-1045-2021>, 2021.
- 653 Shobe, C. M., Tucker, G. E., and Barnhart, K. R.: The SPACE 1.0 model: A Landlab component for 2-D calculation of
654 sediment transport, bedrock erosion, and landscape evolution, *Geosci. Model Dev. Discuss.*, 1–38,
655 <https://doi.org/10.5194/gmd-2017-175>, 2017.



- 656 Starke, J., Ehlers, T. A., and Schaller, M.: Latitudinal effect of vegetation on erosion rates identified along western South
657 America, *Science*, 367, 1358–1361, <https://doi.org/10.1126/science.aaz0840>, 2020.
- 658 Steegen, A., Govers, G., Nachtergaele, J., Takken, I., Beuselinck, L., and Poesen, J.: Sediment export by water from an
659 agricultural catchment in the Loam Belt of central Belgium, *Geomorphology*, 33, 25–36, [https://doi.org/10.1016/S0169-555X\(99\)00108-7](https://doi.org/10.1016/S0169-555X(99)00108-7), 2000.
- 661 Stephenson, J., Gallagher, K., and Holmes, C.: A Bayesian approach to calibrating apatite fission track annealing models for
662 laboratory and geological timescales, *Geochim. Cosmochim. Acta*, 70, 5183–5200, <https://doi.org/10.1016/j.gca.2006.07.027>,
663 2006.
- 664 Suescún, D., Villegas, J. C., León, J. D., Flórez, C. P., García-Leoz, V., and Correa-Londoño, G. A.: Vegetation cover and
665 rainfall seasonality impact nutrient loss via runoff and erosion in the Colombian Andes, *Reg. Environ. Change*, 17, 827–839,
666 <https://doi.org/10.1007/s10113-016-1071-7>, 2017.
- 667 Tucker, G. E. and Bras, R. L.: A stochastic approach to modeling the role of rainfall variability in drainage basin evolution,
668 *Water Resour. Res.*, 36, 1953–1964, <https://doi.org/10.1029/2000wr900065>, 2000.
- 669 Übernicker, K., Ehlers, T. A., Ershadi, M. R., Paulino, L., Fuentes Espoz, J.-P., Maldonado, A., Osés-Pedraza, R., and von
670 Blanckenburg, F.: Time series of meteorological station data in the EarthShape study areas of in the Coastal Cordillera, Chile,
671 <https://doi.org/10.5880/FIDGEO.2020.043>, 2020.
- 672 Wang, L., Zheng, F., Liu, G., Zhang, X. J., Wilson, G. V., Shi, H., and Liu, X.: Seasonal changes of soil erosion and its spatial
673 distribution on a long gentle hillslope in the Chinese Mollisol region, *Int. Soil Water Conserv. Res.*, 9, 394–404,
674 <https://doi.org/10.1016/j.iswcr.2021.02.001>, 2021.
- 675 Wei, W., Chen, L., Zhang, H., and Chen, J.: Effect of rainfall variation and landscape change on runoff and sediment yield
676 from a loess hilly catchment in China, *Environ. Earth Sci.*, 73, 1005–1016, <https://doi.org/10.1007/s12665-014-3451-y>, 2015.
- 677 Wulf, H., Bookhagen, B., and Scherler, D.: Seasonal precipitation gradients and their impact on fluvial sediment flux in the
678 Northwest Himalaya, *Geomorphology*, 118, 13–21, <https://doi.org/10.1016/j.geomorph.2009.12.003>, 2010.
- 679 Yetemen, O., Istanbuluoglu, E., Flores-Cervantes, J. H., Vivoni, E. R., and Bras, R. L.: Ecohydrologic role of solar radiation
680 on landscape evolution, *Water Resour. Res.*, 51, 1127–1157, <https://doi.org/10.1002/2014wr016169>, 2015.
- 681 Zhang, S., Li, Z., Hou, X., and Yi, Y.: Impacts on watershed-scale runoff and sediment yield resulting from synergetic changes
682 in climate and vegetation, *Catena*, 179, 129–138, <https://doi.org/10.1016/j.catena.2019.04.007>, 2019.
- 683 Zhang, W., An, S., Xu, Z., Cui, J., and Xu, Q.: The impact of vegetation and soil on runoff regulation in headwater streams on
684 the east Qinghai–Tibet Plateau, China, *Catena*, 87, 182–189, <https://doi.org/10.1016/j.catena.2011.05.020>, 2011.
- 685 Zhang, X., Yu, G. Q., Li, Z. B., and Li, P.: Experimental Study on Slope Runoff, Erosion and Sediment under Different
686 Vegetation Types, *Water Resour. Manag.*, 28, 2415–2433, <https://doi.org/10.1007/s11269-014-0603-5>, 2014.
- 687 Zheng, F. L.: Effect of Vegetation Changes on Soil Erosion on the Loess Plateau I Project supported by the Chinese Academy
688 of Sciences (No. KZCX3-SW-422) and the National Natural Science Foundation of China (Nos. 9032001 and 40335050).,
689 *Pedosphere*, 16, 420–427, [https://doi.org/10.1016/S1002-0160\(06\)60071-4](https://doi.org/10.1016/S1002-0160(06)60071-4), 2006.
- 690 Ziese, M., Rauthe-Schöch, A., Becker, A., Finger, P., Rustemeier, E., and Schneider, U.: GPCC Full Data Daily Version 2020
691 at 1.0°: Daily Land-Surface Precipitation from Rain-Gauges built on GTS-based and Historic Data: Gridded Daily Totals
692 (2020), https://doi.org/10.5676/DWD_GPCC/FD_D_V2020_100, 2020.
- 693